Energy Release Rate Cannot Predict Crack Initiation Orientation in Domains with a Sharp V-notch Under Mode III Loading

Brigit Mittelman and Zohar Yosibash

Pearlstone Center for Aeronautical Engineering Studies, Dept. of Mechanical Engineering Ben-Gurion University of the Negev, Beer-Sheva, 84105, Israel

Abstract

The energy release rate (ERR) proposed by Irwin based on a theory by Griffith [1, 2] has been extensively used as a fracture criterion in 2D for brittle domains. Under in-plane mixed mode loading (modes I+II), the direction of crack initiation from cracks and sharp V-notches was determined by the orientation at which the ERR attains its maximum.

Using the newly developed asymptotic expansion presented in [3] verified by direct results from finite element analyses we demonstrate that the ERR under mode III cannot predict the fracture initiation direction correctly. The ERR maximum value is always obtained along the V-notch bisector, contrary to experimental observations. This forbids the ERR to be applied as a failure initiation criterion in cases where mode III is dominant.

Keywords: Potential Energy, V-notch, failure criterion, 3D singularities

1. Introduction

Most failure initiation criteria in elastic brittle homogeneous and isotropic structures containing sharp V-notches or cracks can be divided into two fundamental approaches: energy-based, and stress-based. One of the most addressed energy approaches utilizes the critical energy release rate (ERR) concept which proposed by Irwin based on a theory by Griffith [1, 2]: A crack initiates in a direction along which the ERR is maximum, and initiation occurs when the ERR reaches a critical value considered a material property. According to the maximum stress criterion, the failure initiation is determined by the maximum normal stress (proposed by Erdogan and Sih [4] for isotropic materials). Failure occurs in the direction perpendicular to the maximum normal stress, and initiation will occur when the stress intensity factor for a crack along this direction reaches a critical value, which is considered a material property.

The present work focuses on the ability of the ERR criterion to predict crack initiation direction from a V-notch under mode III loading in the context of finite fracture mechanics (examples for the FFM approach in 2D can be found in [5, 6]). There are several experimental results available of quasi-brittle materials under loading conditions which involve mode III. A common geometry used in these experiments is a cylindrical rod with a circumferential notch, loaded in torsion. Examples for such experiments include Alumina [7] (Fig. 1), and PMMA [8, 9] (Fig. 2). The fracture surfaces are of complicated and segmented shapes, and individual crack initiation sites along the original crack edge can be observed.

Email address: zohary@bgu.ac.il (Brigit Mittelman and Zohar Yosibash)

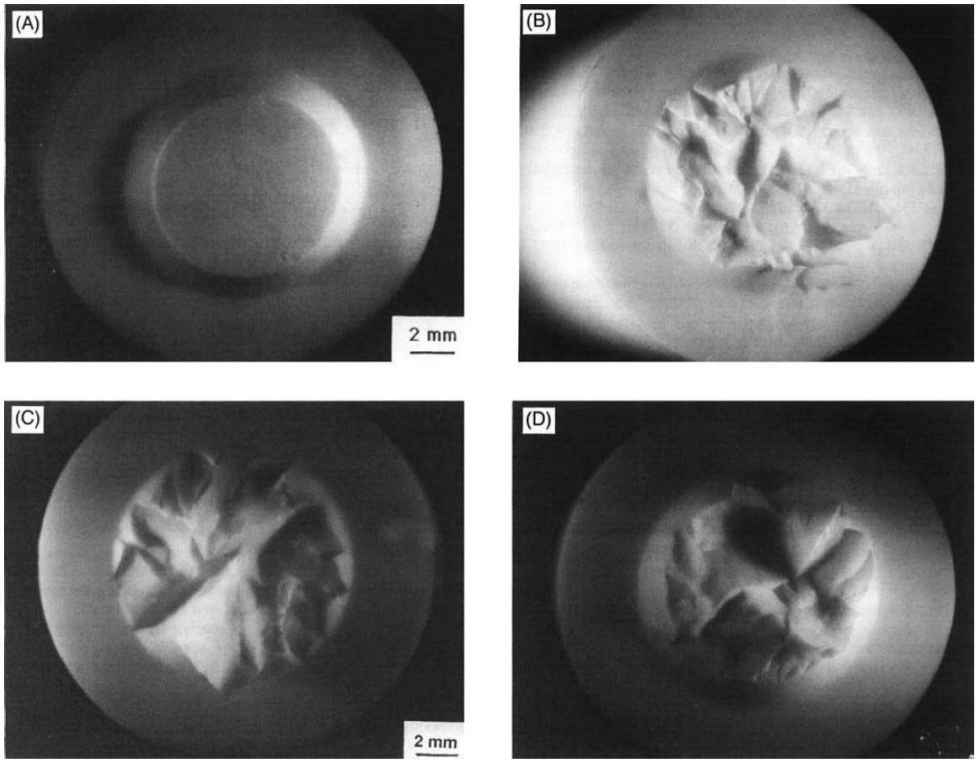

Figure 1: Fracture surfaces from [7] of Alumina cylindrical specimens under (a) pure tension, (b) pure torsion, and (c,d) different combinations of tension and torsion.

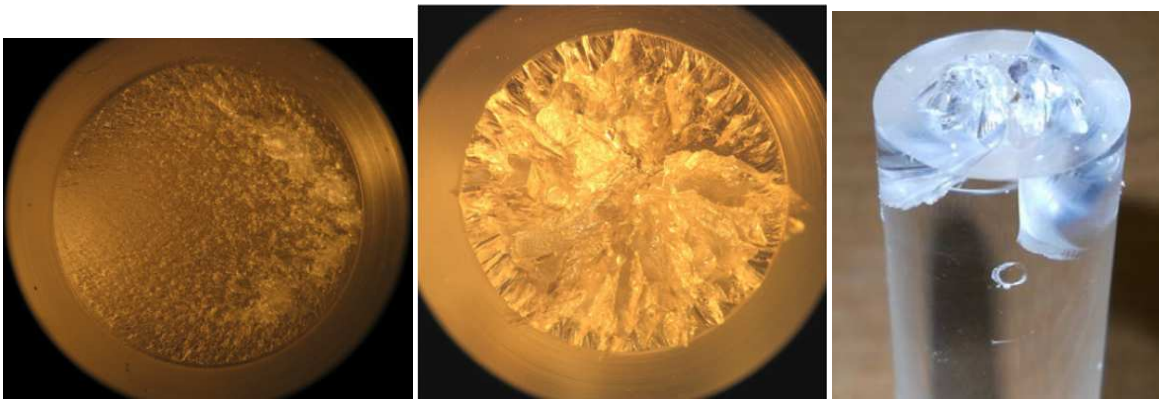

(a) (b) (c)

Figure 2: Fracture surfaces of PMMA cylindrical specimens under pure tension (a), and pure torsion (b) from [9], and under pure torsion from [8] (c).

For straight V-notch edges, only few experimental examples were documented in quasi-brittle materials where mode III was involved. Lazarus et al. [10] have conducted experiments on a slant crack geometry under 3 point bending. We have chosen a similar geometry of PMMA bars with slanted V-notch and loaded them to fracture under 4 point bending (see Fig. 3 (a)). The inclination angle of the notch ($\gamma \neq 0^o$) created a mixed mode I+II+III state of stress along the V-notch front, and a segmented fracture surface (Fig. 3 (c,d)). Knauss [11] applied out-of-plane

shear (Fig. 4 (a)) on a brittle polymer (Solithane 113) with a single edge notch geometry and has observed multiple crack initiation sites distributed along the original crack front, at an angle of 45^o with respect to the original front (Fig. 4 (b)).

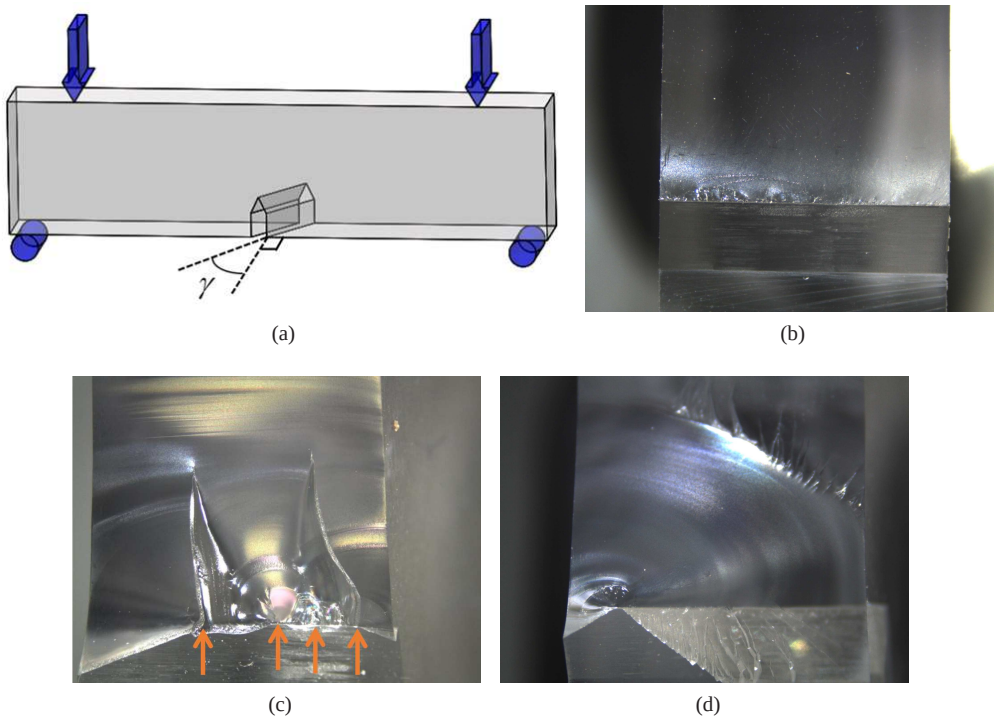

(a) (b)

(c) (d)

Figure 3: Optical fractography (stereoscope, magnification $\times 8$) of specimen surfaces after fracture in 4PB (a) with the same notch height and different inclination angles $\gamma = 0^o$ (b),$\gamma = 30^o$ - the arrows denote crack origins (c),$\gamma = 45^o$ (d).

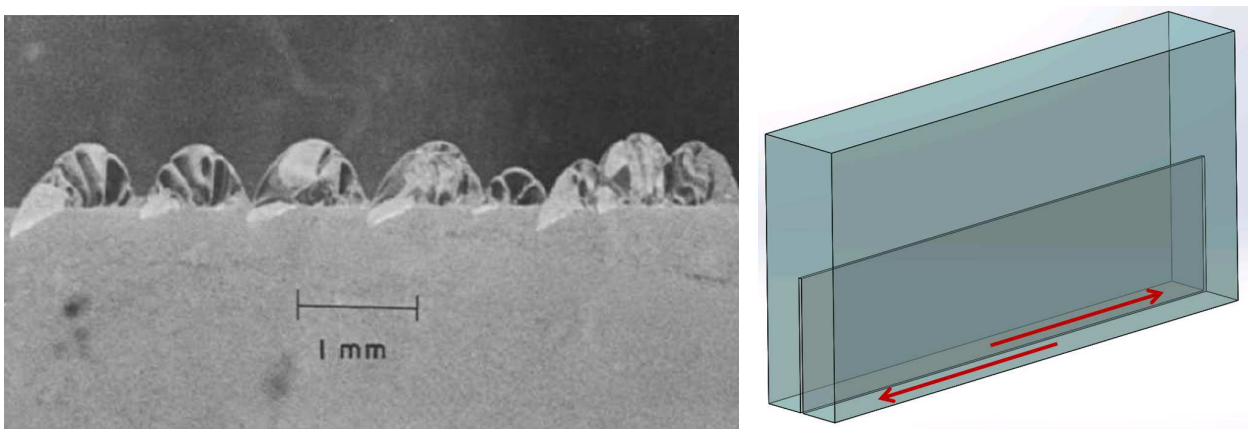

(a) (b)

Figure 4: Fracture surface of a brittle polymer (Solithane 113) after arrested crack growth from [11]. View (a) is normal to the specimen surface. The lower and lighter parts of the picture represent the original crack surface. The specimen geometry and loading are presented schematically in (b).

We address the ability of the ERR to predict crack initiation direction under mode III loading. ERR is defined in classical fracture mechanics as: $\mathcal{G} = \left(-\frac{\partial \Pi}{\partial S}\right) = \lim_{\delta S \to 0} -\frac{\delta \Pi}{\delta S}$, which refers to a crack propagating from an existing crack [1]. It can also be defined in finite fracture mechanics (FFM) as: $\mathcal{G} = -\frac{\delta \Pi}{S}$ (implemented in 2D in [5, 6]) which refers to a small but **finite** crack of area S initiating from a V-notch. We show herein that under mode III loading, neither can predict the crack initiation direction observed by experiments. This is contrary to mode I+II loading, for which both FFM ERR [12, 5] and classical ERR [13] were shown to successfully predict crack initiation direction. This observation has been made for classical ERR by Cooke and Pollard [14], which have used the following relation between the ERR and the Stress Intensity Factors (SIFs) [15]:

$$G(\phi) = K_I^2(\phi)\frac{1-\nu^2}{E} + K_{III}^2(\phi)\frac{1+\nu}{E} \tag{1}$$

Where ϕ is the twist angle of crack facets with respect to initial crack, E is Young's modulus, ν is the Poisson ratio and K_I, K_{III} are the SIFs associated with modes I and III, respectively. However, the validity of their results is questionable since the relation between the ERR and SIFs of the form provided in (1) is obtained under the assumption that a crack under combined loading grows along the initial crack plane [16].

Former fracture initiation criteria involving mode III loading that were based on the energy approach, [17, 10, 18, 13, 19] all involve assumptions that limit their ability to describe a general state of crack initiation, such as in Fig. 3 (c,d). In [18] failure initiation is described by one angle only, and the dependence of the stress intensity factor K_{III} on the coordinate along the crack edge is disregarded. In Lazarus et al. [17] a mesoscopically segmented fracture surface was represented by a macroscopic smoothly twisting crack extension. In the initiation criterion proposed by Lin et al. [20] for cracks under modes I+III, the faceted crack front was characterized by a single angle of fragmentation. Crack initiation criteria under mixed modes I+III is extensively discussed in [21]. The aforementioned crack initiation criteria available for loading conditions which involve mode III cannot be used to characterize fracture surfaces such as observed in Fig. 3 (c,d), where the number, location and orientation of crack origins can change locally throughout the crack edge.

In [3] we have presented an analysis for FFM ERR calculations, which applies to a local finite virtual crack initiation from a V-notch with a straight edge and is utilized in the present work. This expansion applies for all possible crack orientations initiating at any point along the V-notch edge except for the vertices, where the edge intersects the free surface.We have not found FFM ERR calculations in literature for comparison. Classical ERR calculations in the presence of mode III, available by the virtual crack extension (VCE) method [22] or the virtual crack closure integral [23], consider crack extensions within the crack plane. The only example of local ERR calculations known to the authors which has included mode III and has considered crack initiation out of its original plane was presented in [24] for a square cross section bar having a quarter-circular crack under combined mode I+III. A fundamental difference between [24] and the method presented in [3] is that the VCE method requires that the base of the crack extension overlaps with the original crack front. Therefore, it is inadequate for describing a crack initiation such as in Fig. 3 (c,d), where the crack initiation orientation has a single point of intersection with the original notch edge (or several separate points - segmented fracture surfaces).

In the present work we show systematically that the ERR cannot predict the physical observations under dominant mode III loading. This is demonstrated for FFM ERR, for two virtual crack geometries initiating from a straight edge V-notched bar (section 3,3.1). We also demonstrate the invalid use of the classical ERR for a crack that propagates from an existing crack (section 4) and in section 5, the FFM ERR is addressed for a cylindrical rod with a circumferential V-notch under mode III loading.

2. Preliminaries and notations

The ERR in FFM is defined by $-\frac{\delta \Pi}{S}$, where $\delta\Pi$ is the difference in the potential energy between a V-notched domain with and without a small planar virtual crack of a **finite** area S created at its tip (see Fig. 5).

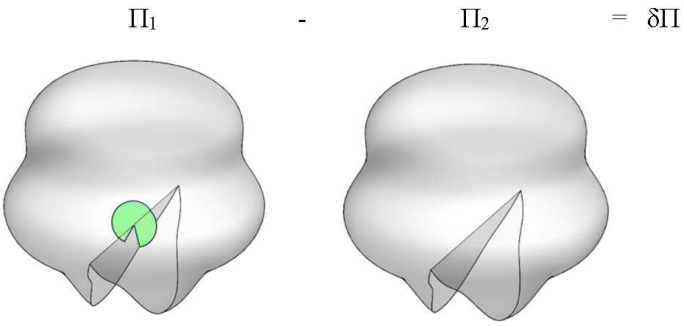

Figure 5: Considered domains for $\delta\Pi$.

$\delta\Pi$ can be computed for any crack orientation (spatial angles α, β) and location along the V-notch edge (z) by [3]:

$$\begin{aligned} -\delta\Pi^{Approx} &= A_1^2 \times (\sqrt{S})^{2\alpha_1+1} H_{11} + A_1 A_2 \times (\sqrt{S})^{\alpha_1+\alpha_2+1}(H_{12}+H_{21}) + A_2^2 \times (\sqrt{S})^{2\alpha_2+1} H_{22} \\ &+ A_1 A_3 \times (\sqrt{S})^{\alpha_1+\alpha_3+1} \times (H_{13}+H_{31}) + A_2 A_3 \times (\sqrt{S})^{\alpha_2+\alpha_3+1}(H_{23}+H_{32}) \\ &+ A_3^2 \times (\sqrt{S})^{2\alpha_3+1} H_{33} + H.O.T. \end{aligned} \tag{2}$$

Or in concise form:

$$-\delta\Pi^{Approx} \approxeq \sum_{i=1}^{3}\sum_{j=1}^{3} A_i(z)\, A_j(z)\, (\sqrt{S})^{\alpha_i+\alpha_j+1}\, H_{ij}(\alpha,\beta) \tag{3}$$

Where $A_i \equiv A_i(z)$ are the general edge stress intensity functions (GESIFs) associated with the V-notch edge at a point z along it (coinciding with the z axis in a Cartesian coordinate representation, see Fig. 6), and the functions $H_{ij}(\alpha,\beta)$ are computed and tabulated, H_{ij} depend on the crack orientation, shape, V-notch opening angle and material properties. H_{ij} has units of $\frac{\text{mm}^2}{\text{N}}$, as can be derived from (3). α_i are the elastic field eigenvalues associated with each loading mode, so that α_1 and α_2 correspond to mode I and II of the 2D in-plane elastic solution and α_3 corresponds to an out-of-plane solution (see [3]). For a crack for example $\alpha_1 = \alpha_2 = \alpha_3 = 1/2$, whereas for a V-notch these depend on the V-notch opening angle ω (see e.g. [25]). Note that the eigenvalues α_i which appear in the exponent of $\sqrt{S}$ need not be confused with the angle α used to define the orientation within the term $H_{ij}(\alpha,\beta)$.

For the case of pure mode III, (3) reduces to:

$$-\delta\Pi^{Approx} \approxeq A_3^2\, (\sqrt{S})^{2\alpha_3+1}\, H_{33}(\alpha,\beta) \tag{4}$$

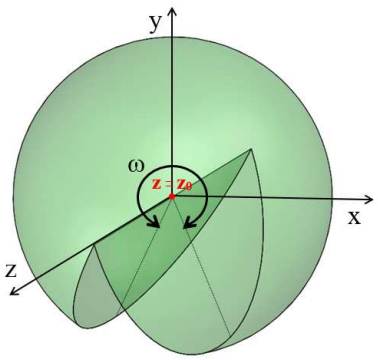

Figure 6: Spherical coordinates representation.

According to the ERR approach the crack is expected to initiate along a direction (α, β) at which $\frac{\delta \Pi}{S}$ attains its maximum [5].

2.1. H_{ij}'s

In 3D we use two angles to describe the spatial orientations of a newly generated crack. These are chosen relative to the V-notch bi-sector plane at the point of crack origin (yz plane in Fig. 6). The angle α describes counter-clockwise rotation around the y axis, and the angle β describes counter-clockwise rotation around the z axis. Since the rotation by α and β is not commutative, we define the rotation (starting from the yz plane, with normal (100)) first by β and then by α. Examples for several circular planes are presented in Fig. 7.

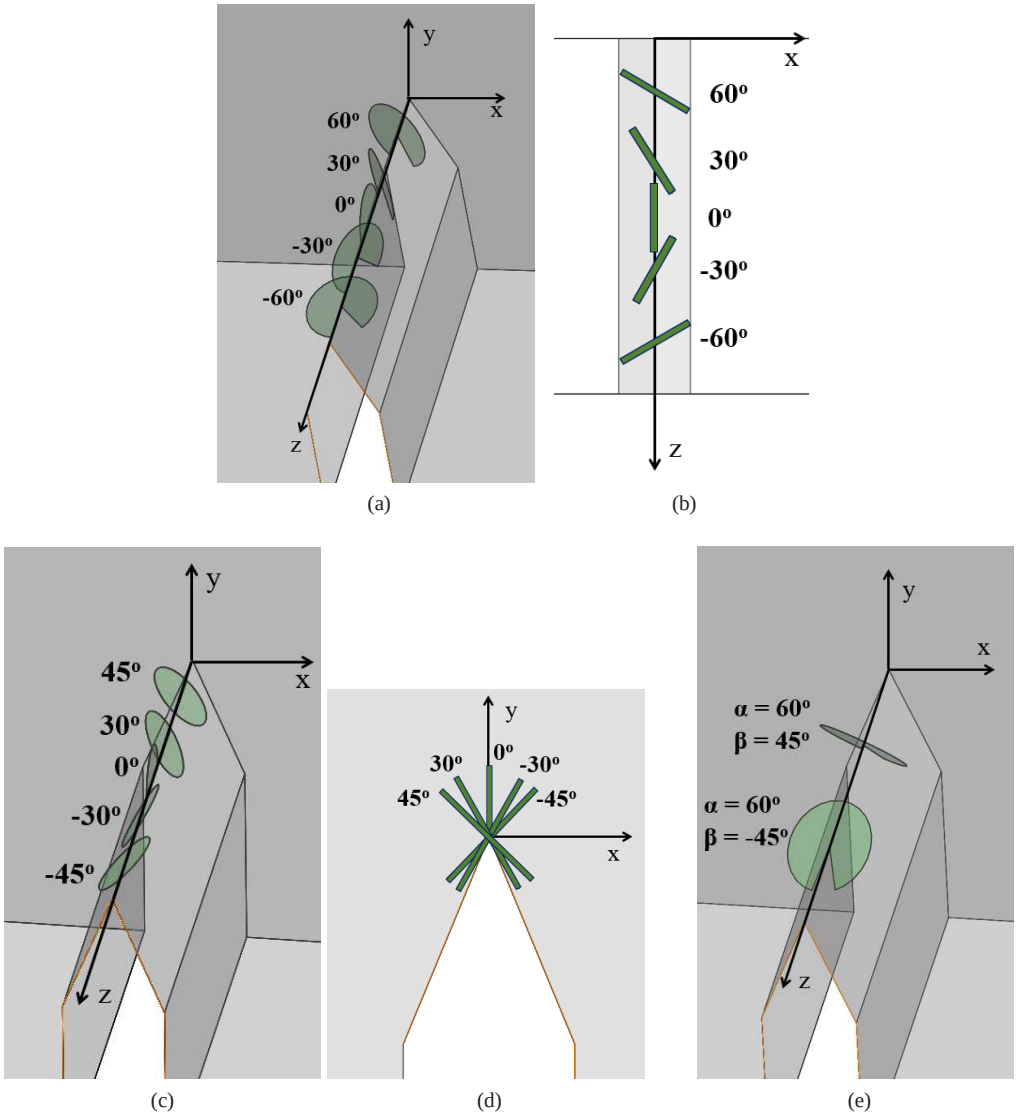

Figure 7: Circular planes obtained for various α, β angles. Rotation by α only: $\alpha = \{60^o, 30^o, 0^o, -30^o, -60^o\}, \beta = 0^o$ (a) isometric view and (b) top view. Rotation by β only: $\alpha = 0^o, \beta = \{45^o, 30^o, 0^o, -30^o, -45^o\}$ from (c) isometric viw and (d) front view. (e) Rotation by $\alpha = 60^o, \beta = \{45^o, -45^o\}$. The planes are presented within a specimen with $\gamma = 0^o$. The cracks were schematically emphasized in (b) and (d) however they represent zero thickness cracks.

$H_{ij}(\alpha,\beta)$ were computed using methods in [3] for a planar crack of circular shape (crack center coincides with the V-notch edge), and a V-notch solid angle $\omega = 315^o = 360^o -$ opening angle (so the opening angle is 45^o). For angles within the range $-60^o \leq \alpha \leq 60^o$ and $-45^o \leq \beta \leq 45^o$, H_{ij} was calculated for discrete orientations (combinations of α, β taken in intervals). PMMA material properties $E = 3900$ MPa, $\nu = 0.332$ were used. Based on these results, a smooth function was chosen to describe the $H_{ij}(\alpha,\beta)$ surfaces optimally. In the present article we concentrate on approximately pure mode III conditions and therefore present only the results for $H_{33}(\alpha,\beta)$.

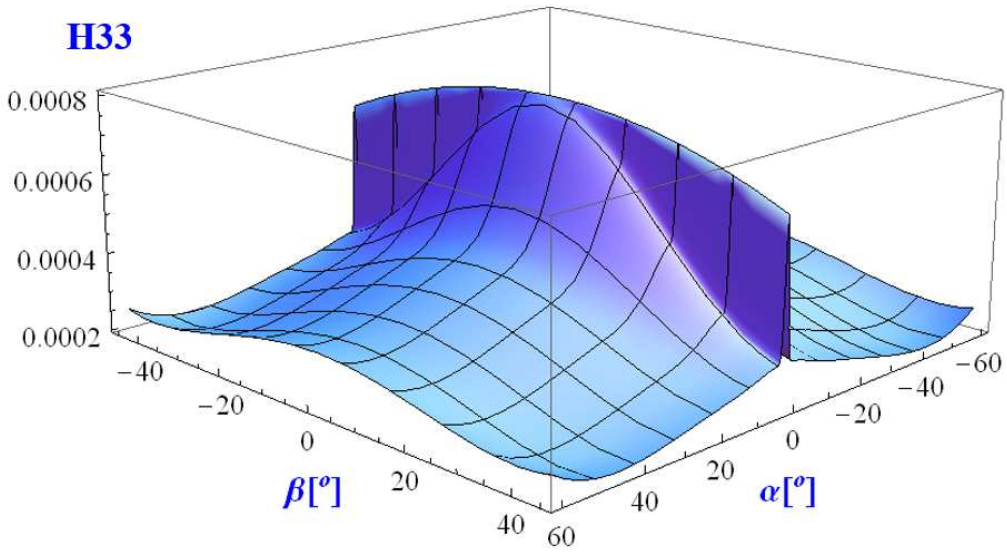

Figure 8: $H_{33}(\alpha,\beta)$ surface approximation for $E = 3900$ MPa, $\nu = 0.332$, $\omega = 315^o$ and circular crack shape.

For a V-notch solid angle of $\omega = 315^o$ and $E = 3900$ MPa, $\nu = 0.332$ the H_{33} surface (Fig. 8) can be approximated by the following function:

$$\begin{aligned} H_{33}(\alpha,\beta,\omega=315^o) &= 0.00046 - 1.07\cdot 10^{-7}\alpha^2 - 1.69\cdot 10^{-7}\beta^2 + 1.96\cdot 10^{-11}\alpha^4 + 1.52\cdot 10^{-11}\alpha^2\beta^2 + 3.87\cdot 10^{-11}\beta^4 \\ &+ 0.00034\, exp[-\frac{\alpha^2}{75}]\, exp[-\frac{\beta^2}{800}] + \left(0.00034 - 0.00034\, exp[-\frac{\beta^2}{800}] + 9.54\cdot 10^{-8}\beta^2 - 3.87\cdot 10^{-11}\beta^4\right)\cdot exp[-\frac{\alpha^2}{0.5}] \end{aligned} \quad (5)$$

The V-notch surfaces are traction-free, so for a V-notch angle of $\omega = 315^o$, $\alpha_3 = 0.5714286$ [3].

3. Crack initiation angle by maximum $\frac{\delta\Pi}{S}$ for mode III loading

Consider for example a bar of dimensions $10 \times 5 \times 10\,\text{mm}^3$ that contains a V-notch (Fig. 9). To obtain a dominant mode III loading, we applied a force of $20000\,N$ in the z direction on the left face, force of -20000 N in the z direction on the right face, force of -20000 N in the x direction on the the front face and finally a force of 20000 N in the x direction on the back face. The lower face was constrained in the y direction, and the right and left faces were constrained in the x direction. $E = 3900$ MPa, $\nu = 0.332$ were used. $A_i(z)$ extracted by the QDFM [26] are shown in Fig. 10. One can observe that A_1, A_2 are negligible compared to A_3. At the center of the V-notch A_1, A_2 are almost zero (three orders of magnitude smaller compared to A_3). Therefore cracks that may initiate at the center of the V-notch edge ($z = 5$ mm) are considered. Different crack orientations and sizes were examined with a circular crack shape. To demonstrate that $\delta\Pi^{Approx}$ well represent $\delta\Pi$, we also computed $\delta\Pi^{FE}$ in two models with identical mesh, so that the crack was defined as two separate surfaces, and in the V-notched model without the crack

the surfaces were merged. The identical meshes ensure that the numerical errors associated with mesh away from the crack "cancel" each when computing

$$\delta\Pi^{FE} \triangleq \Pi^{FE}_{V-notch+crack} - \Pi^{FE}_{V-notch} \tag{6}$$

$\delta\Pi^{Approx}$ was also calculated using H_{33} data from Fig. 8 and tabulated in Table 1.

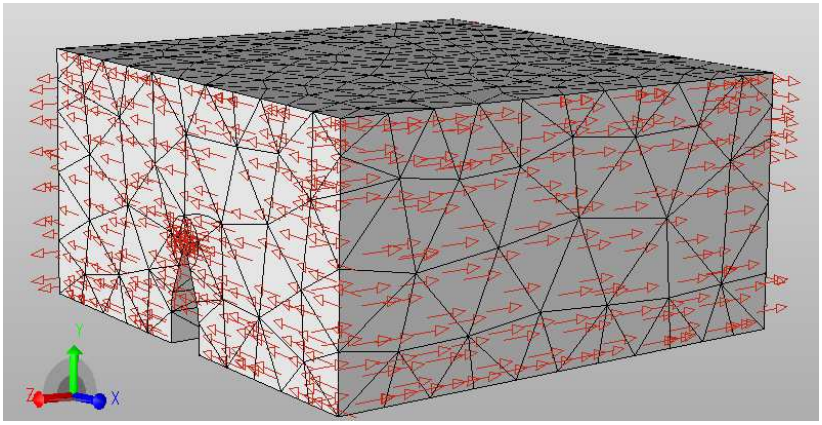

Figure 9: The FE model used for the mode III loading example.

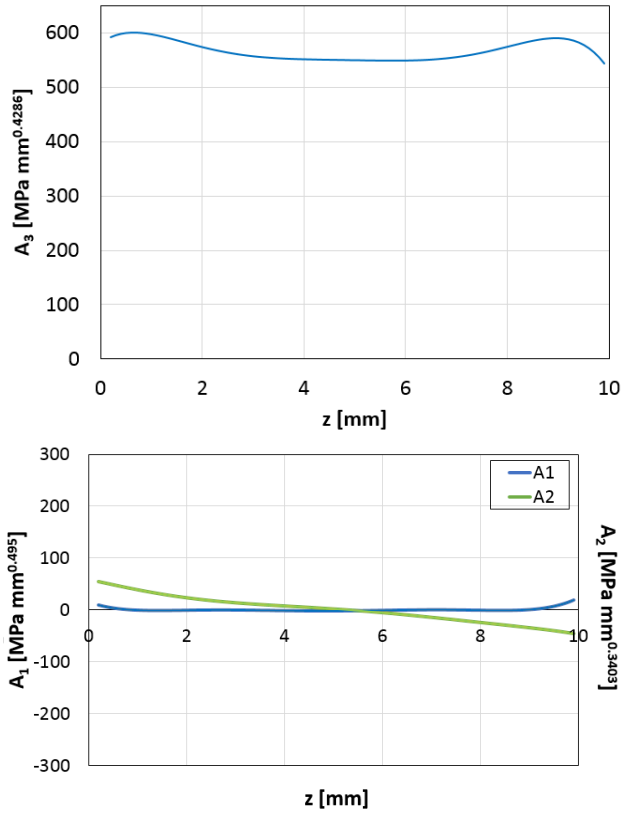

Figure 10: $A_1(z)$, $A_2(z)$, and $A_3(z)$ for the $10 \times 5 \times 10$ mm bar in Fig. 9 with a V-notch of $\omega = 315^\circ$ under mode III loading.

crack orientation	crack area mm^2	Π^{FE} $p \to \infty$ N mm	error in energy norm at p=7	$\delta\Pi^{FE}$ N mm from FE models	$\delta\Pi^{Approx}$ N mm	% difference between $\delta\Pi^{FE}$ and $\delta\Pi^{Approx}$
no crack		-32260.79	1.17%			
$\alpha = 0^o$ $\beta = 0^o$	**0.05**	-32270.83	1.18%	**-10.03**	**-9.76**	-2.7%
no crack		-32261.7	1.18%			
$\alpha = 0^o$ $\beta = 0^o$	0.07	-32276.14	1.14%	-14.43	-14.77	-2.4%
no crack		-32261.72	1.16%			
$\alpha = 0^o$ $\beta = 0^o$	0.1	-32282.92	1.21%	-21.2	-20.4	-3.8%
no crack		-32261.72	1.13%			
$\alpha = 30^o$ $\beta = 0^o$	**0.05**	-32266.03	1.14%	**-4.3**	**-4.22**	-1.8%
no crack		-32261.74	1.19%			
$\alpha = 45^o$ $\beta = 0^o$	**0.05**	-32265.62	1.19%	**-3.87**	**-3.82**	-1.24%
no crack		-32261.76	1.23%			
$\alpha = 45^o$ $\beta = 0^o$	0.07	-32267.56	1.24%	-5.8	-5.49	-5.3%
no crack		-32261.74	1.19%			
$\alpha = 45^o$ $\beta = 0^o$	0.1	-32269.92	1.21%	-8.18	-8.04	-1.7%

Table 1: $\delta\Pi^{FE}$ results compared to $\delta\Pi^{Approx}$ for the $10 \times 5 \times 10$ mm V-notched bar under mode III loading

The difference between $\delta\Pi^{Approx}$ and $\delta\Pi^{FE}$ for the mixed mode loading is less than 4%. The $\delta\Pi^{Approx}$ expression was validated for a variety of crack orientations, shapes, sizes and boundary conditions.

Experimental evidence suggests that under dominant mode III as in Fig. 9, the virtual crack initiates at an angle of about $(\alpha, \beta) \sim (45^o, 0^o)$, i.e. that $\delta\Pi$ will be maximal in this orientation. However, $\delta\Pi^{FE}$ (and the respective $\delta\Pi^{Approx}$, as well as FFM ERR) attains its maximum in the direction of the V-notch bisector $(\alpha, \beta) = (0^o, 0^o)$. This result can be foreseen from the asymptotic expansion of $\delta\Pi^{Approx}$ when one considers that under pure mode III loading, $\delta\Pi^{Approx}$ reduces to $-A_3^2(z_0) \times (\sqrt{S})^{2\alpha_3+1} \times H_{33}$ (4). For a specific location z and choice of crack area S, $\delta\Pi^{Approx}$ is determined solely by H_{33}, and the shape of $H_{33}(\alpha, \beta)$ in Fig. 8 clearly shows maximum values at $(\alpha, \beta) = (0^o, 0^o)$ for spatial orientations in the range $-60^o \leq \alpha \leq 60^o$ and $-45^o \leq \beta \leq 45^o$. This clearly indicates that the energy release rate consideration in FFM cannot independently predict the physical observations and may not be used independently as a criterion for failure initiation.

3.1. $\delta\Pi$ for different crack geometries under mode III loading

One could assume that the conclusions in the previous section are due to the FFM assumptions, i.e. are a result of the abrupt change of crack shape from half a circle at $\alpha \sim 0^o$ to a circular sector at $\alpha \neq 0^o$. Specifically, the abrupt change from an intersection **line** between the virtual crack and the V-notch edge at $\alpha = 0^o$ (the circle diameter) to an intersection **point** between them at $\alpha \neq 0^o$ (the circle's center). Therefore, $\delta\Pi^{FE}$ was examined for a crack geometry of a medallion - a circle which has a single point of intersection between its circumference and the V-notch edge, at any orientation. The radius of the circular crack was 0.2 mm. As previously described, $\delta\Pi^{FE}$ was calculated by $\delta\Pi^{FE} \triangleq \Pi^{FE}_{V-notch+crack} - \Pi^{FE}_{V-notch}$ where the two FE models (V-notched with and without a crack) were meshed identically. The external geometry, loading and boundary conditions were as in Fig. 9. The only difference is the crack orientation, as presented in Fig. 11. The $\delta\Pi^{FE}$ results are summarized in Table 2.

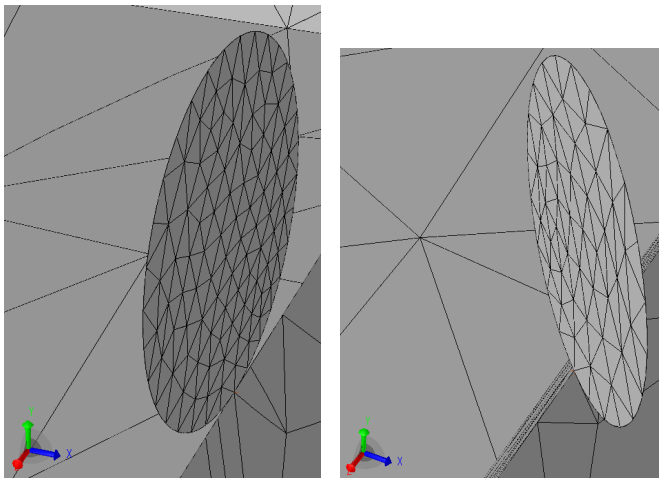

(a) (b)

Figure 11: "Medallion" crack geometry at (a) $(\alpha, \beta) = (0^o, 0^o)$ and (b) $(\alpha, \beta) = (45^o, 0^o)$ orientations.

crack orientation	crack area mm^2	Π^{FE} $p \to \infty$ N mm	error in energy norm at p=7	$\delta\Pi^{FE}$ N mm from FE models
no crack		-32261.72	1.14%	-9.8
$\alpha = 0^o$ $\beta = 0^o$	0.125	-32271.52	1.19%	
no crack		-32261.55	1.18%	-7.07
$\alpha = 45^o$ $\beta = 0^o$	0.125	-32268.62	1.21%	

Table 2: $\delta\Pi^{FE}$ results for $10 \times 5 \times 10$ mm V-notched bar under dominant mode III loading and "medallion" crack shape.

One notices, that also for the "medallion" crack with a single point of intersection at any angle (α, β), $\delta\Pi^{FE}$ (and FFM ERR) is larger for a crack at the V-notch bisector under dominant mode III loading.

4. Classical ERR approach for mode III loading

In section 3 we have considered a bar specimen with a V-notch under dominant mode III loading (Fig. 10). $\delta\Pi$ was compared for different crack orientations and sizes. The FFM ERR $\mathcal{G} = -\frac{\delta\Pi^{FE}}{S}$ which refers to a **finite** crack initiation from a V-notch, is maximum at the V-notch bisector orientation $(\alpha, \beta) = (0^o, 0^o)$, contrary to experimental observations for dominant mode III fractures.

Using the results from Table 1 one can also calculate the classical ERR, which is defined for crack propagation from an existing crack. Taking geometry with a smaller crack as a reference, classical ERR was calculated along the initial crack plane (Table 3).

crack orientation	original crack area mm^2	$\delta\Pi^{FE}$ N mm from FE models	$\delta\Pi^{FE}$ N mm	δS mm^2	$\mathcal{G} = -\frac{\delta\Pi^{FE}}{\delta S}$ N mm
$\alpha = 0^o$ $\beta = 0^o$	0.05	-10.03			
$\alpha = 0^o$ $\beta = 0^o$	0.07	-14.43	-4.4	0.02	220
$\alpha = 0^o$ $\beta = 0^o$	0.1	-21.2	-6.67	0.03	222.33
$\alpha = 45^o$ $\beta = 0^o$	0.05	-3.87			
$\alpha = 45^o$ $\beta = 0^o$	0.07	-5.8	-1.93	0.02	96.5
$\alpha = 45^o$ $\beta = 0^o$	0.1	-8.18	-2.38	0.03	79.3

Table 3: Classical ERR calculations for crack initiation from an existing crack taken as the reference (initial condition). Calculations are based on data from Table 1.

One notices in Table 3, that the classical ERR along the V-notch bisector plane orientation $(\alpha, \beta) = (0^o, 0^o)$ is larger compared with the slanted orientation $(\alpha, \beta) = (45^o, 0^o)$ under dominant mode III loading. These results agree with those obtained for the FFM ERR (Table 1).

5. FFM ERR for a cylindrical rod with a circumferential V-notch under torsion

Cylindrical rods with circumferential notch under torsion are extensively used in literature for mode III experiments [8, 9, 7, 11]. These experiments have shown that the crack initiation plane under dominant mode III is approximately at -45^o to the notch bisector $(\alpha, \beta) \sim (-45^o, 0^o)$. Therefore, we have calculated $\delta\Pi^{FE}$ because of a crack in the $(\alpha, \beta) = (0^o, 0^o)$ and $(\alpha, \beta) = (-45^o, 0^o)$ planes. $\delta\Pi^{FE}$ was obtained by (6), so for each geometry two FE models were constructed - with and without a crack, identically meshed. The specimen's geometry was as presented in Fig. 12 (a) (matches one of the specimens in [8]). Force of 1000 N was applied in the θ direction on the upper face, force in the opposite direction (-1000 N in the θ direction) was applied on the lower face. PMMA material properties $E = 3900$ MPa, $\nu = 0.332$ were used. The cracks geometry was similar to a quarter circle (Fig. 12 (b,c)), resembling the shapes observed in the fracture surface in Fig. 2 (b,c). The results are presented in Table 4.

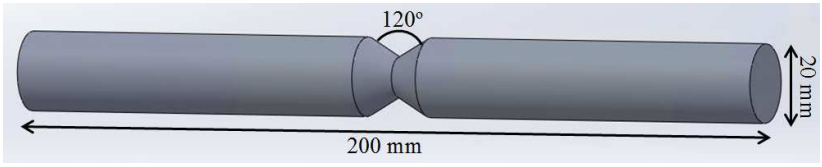

(a)

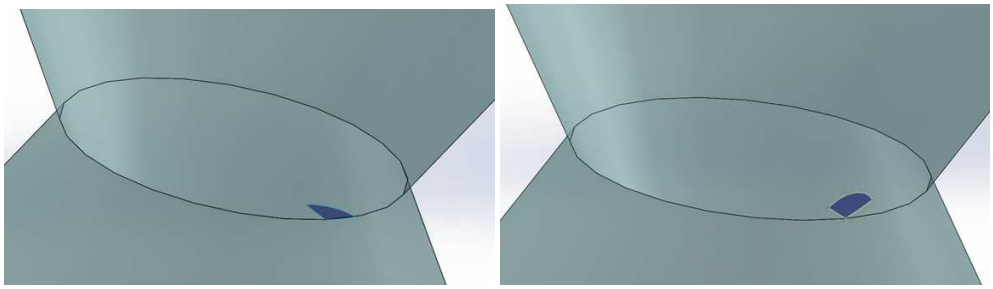

(b) (c)

Figure 12: Cylindrical rod dimensions and geometry (a). Planar crack in the notch bisector plane (b) (blue crack inside grey cylinder, view of the central region of the cylinder), planar crack in 45^o to the notch bisector (c).

crack orientation	crack area S mm^2	Π^{FE} $p \to \infty$ N mm	error in energy norm at p=7	$\delta\Pi^{FE}$ N mm from FE models	$\mathcal{G} = -\frac{\delta\Pi^{FE}}{S}$ $\frac{\text{N}}{\text{mm}}$
no crack		-268.304	2.08%	-0.173	0.216
$\alpha = 0^o$ $\beta = 0^o$	0.8	-268.476	2.1%		
no crack		-268.343	2.04%	-0.109	0.137
$\alpha = -45^o$ $\beta = 0^o$	0.8	-268.452	2.05%		

Table 4: $\delta\Pi^{FE}$ results for cylindrical rod (described in Fig. 12) with circumferential notch under torsion, with and without single cracks.

One may observe that although experimental observations show crack initiation sites at approximately -45^o to the notch bisector plane, $\delta\Pi^{FE}$ calculations show larger $\delta\Pi^{FE}$ at the notch bisector than at the plane -45^o to it. Since the crack area and shape were identical at both cases, the FFM ERR is larger as well at the notch bisector. This is again contrary to expectations since ERR is thought to be maximum at the crack initiation orientation.

For the same geometry and loading conditions, we have also examined a case in which eight cracks of the same shape and size as before (quarter circles) are simultaneously present, at equal distances from each other. Another example examined was of tightly located cracks, resulting in 30 cracks along the V-notch edge. These are better approximations to the fracture surfaces in Figures 1 and 2. The same orientations as before were chosen - so that all cracks are along the notch bisector plane or at -45^o to that plane (see Fig. 13).

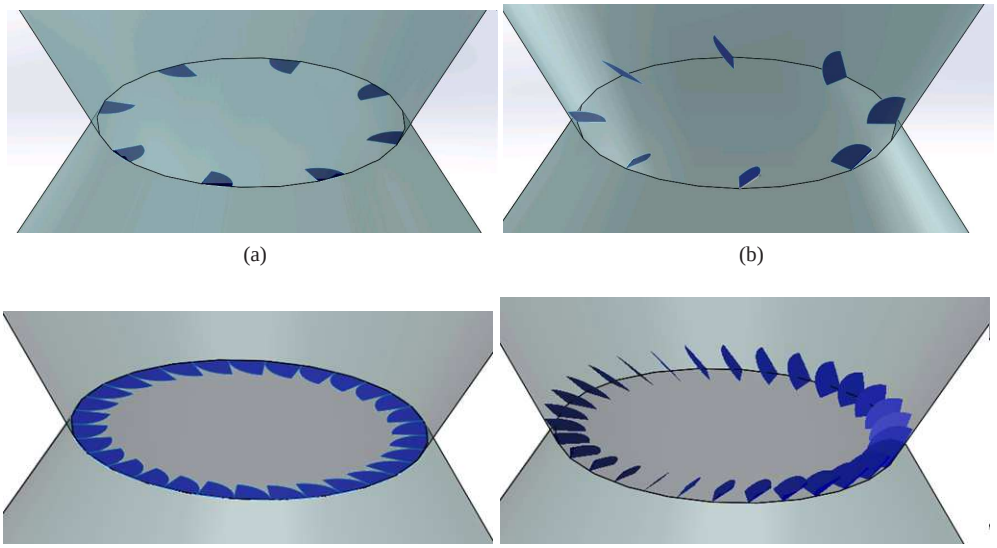

(a) (b)

(c) (d)

Figure 13: 8 planar cracks in the notch bisector plane (a) (blue cracks inside grey cylinder), and planar cracks at -45^o to the notch bisector (b). Tightly located 30 cracks along the same $\alpha = 0^o$ (c) and $\alpha = -45^o$ (d) planes.

crack orientation	crack area S mm^2	Π^{FE} $p \to \infty$ N mm	error in energy norm at p=7	$\delta\Pi^{FE}$ N mm from FE models	$\mathcal{G} = -\frac{\delta\Pi^{FE}}{S}$ $\frac{\text{N}}{\text{mm}}$
no crack		-267.827	2.4%	-1.4	0.219
$\alpha = 0^o$ $\beta = 0^o$	6.4	-269.226	2.47%		
no crack		-267.979	1.72%	-0.88	0.138
$\alpha = -45^o$ $\beta = 0^o$	6.4	-268.864	1.8%		

Table 5: $\delta\Pi^{FE}$ results for cylindrical rod (described in Fig. 13) with circumferential notch under torsion, with and without multiple (8) cracks.

crack orientation	crack area S mm^2	Π^{FE} $p \to \infty$ N mm	error in energy norm at p=6	$\delta\Pi^{FE}$ N mm from FE models	$\mathcal{G} = -\frac{\delta\Pi^{FE}}{S}$ N mm
no crack		-267.309	0.88%	-9.61	0.401
$\alpha = 0^o$ $\beta = 0^o$	24	-276.921	4.55%		
no crack		-267.859	2.01%	-3.51	0.146
$\alpha = -45^o$ $\beta = 0^o$	24	-271.368	2.77%		

Table 6: $\delta\Pi^{FE}$ results for cylindrical rod (described in Fig. 13) with circumferential notch under torsion, with and without tightly located multiple (30) cracks.

One may observe the $\delta\Pi^{FE}$ and therefore FFM ERR are larger at $(\alpha, \beta) = (0^o, 0^o)$ (notch bisector) compared to the $(\alpha, \beta) = (-45^o, 0^o)$ plane, independently of the number of cracks. No mutual influence between the cracks is observed for cracks on the $(\alpha, \beta) = (-45^o, 0^o)$ plane, so that the ERR remains similar for this orientation, for both individual and multiple cracks. At the $(\alpha, \beta) = (0^o, 0^o)$ plane, ERR is similar for 1 and 8 cracks and increases for the tightly located cracks (Tables 4-6). In all cases examined ERR along $(0^o, 0^o)$ is larger than along $(-45^o, 0^o)$, and even more so in the example with the 30 cracks, which is the closest representation to the fracture surface in Fig. 2.

6. Summary and conclusions

Using the newly developed asymptotic expansion presented in [3] as well as direct results from FE analyses we showed that the direction of maximum ERR under mode III loading does not agree with experimental observations. The crack initiation orientation $(\alpha, \beta) \simeq (45^o, 0^o)$, as evident from the various experiments documented in the literature and our own experiments, cannot be predicted by the maximum ERR direction which is obtained at $(\alpha, \beta) = (0^o, 0^o)$. This discrepancy was shown for both FFM ERR (for crack initiation from a V-notch) and classical ERR (for crack initiation from an existing crack). The abrupt change in crack orientation in relation to the V-notch edge seems energetically non preferable. Therefore, both FFM and classical ERR may not be used as a criterion for failure initiation orientation when mode III loading is involved.

Although we have presented only cracks shaped as circular sectors (assumed as the virtual crack initiators), we have also performed several preliminary studies in which elliptical shaped initial cracks were investigated. In these studies we observed the same trend, i.e. using the ERR criterion the crack initiation is preferred along the V-notch bi-sector.

Thus we conclude that the ERR in either FFM or classical fracture mechanics framework is inappropriate as an independent criterion to predict the direction at which fracture evolves under a mode III dominant load.

It is important to note that the maximum normal stress in the close vicinity of the V-notch edge, under mode III dominant load does coincide with the crack initiation direction observed experimentally $(\alpha, \beta) \simeq (45^o, 0^o)$. This result has been obtained by calculating the normal stress over a constant circular area and under a constant force: $\int \sigma_n(r_p, \theta_p)\, r_p\, dr_p\, d\theta_p$, for various orientations (α, β) going through the same point located along the V-notch edge. (r_p, θ_p) are polar coordinates defined on each chosen plane. Out of all the orientations examined, (α, β) for which the result of this integral was maximum was approximately $(\alpha, \beta) \simeq (45^o, 0^o)$ under mode III loading. This calculation actually provides an average normal stress, since the same area is taken for all orientations. We have also confirmed the orientation (α, β) for which the normal stress is maximum does not change with applied force or for different areas of integration (as long as they are kept small). This suggested alternative for determining the crack initiation orientation will be discussed and detailed in a following paper.

Thus, unlike the situation observed under a combined mode I+II loading, where both the ERR and maximum stress criterion resulted in the same crack initiation direction, in a dominant mode III loading these two criteria yield different outcomes.

Acknowledgements: The authors thank Dr. Netta Omer for the computer program for GESIFs computations. This research was supported by the Israel Science Foundation (grant No. 593/14).

References

[1] A. A. Griffth. The phenomena of rapture and flow in solids. *Philosophical Transactions Series A*, 221:163–198, 1920.

[2] G.R. Irwin. Analysis of stresses and strains near the end of a crack traversing a plate. *Journal of Applied Mechanics*, 24:361–364, 1957.

[3] B. Mittelman and Z. Yosibash. Asymptotic analysis of the potential energy difference because of a crack at a V-notch edge in a 3D domain. *Engineering Fracture Mechanics*, 131:232–256, 2014.

[4] F. Erdogan and G. Sih. On the crack extention in plates under loading and transverse shear. *Journal of Basic Engineering*, 85:519–527, 1963.

[5] D. Leguillon. Strength or toughness? a criterion for crack onset at a notch. *European Journal of Mechanics and Solids*, 21:61–72, 2002.

[6] A. Carpinteri, P. Cornetti, N. Pugno, A. Sapora, and D. Taylor. A finite fracture mechanics approach to structures with sharp V-notches. *Engineering Fracture Mechanics*, 75:1736–1752, 2008.

[7] S. Suresh. Combined mode I-mode III fracture of fatigue-precracked alumina. *Journal of American Ceramic Society*, 70:726–733, 1987.

[8] F. Berto, D.A. Cendon, P. Lazzarin, and M. Elices. Fracture behaviour of notched round bars made of PMMA subjected to torsion at -60c. *Engineering Fracture Mechanics*, 102:271–287, 2013.

[9] L. Susmel and D. Taylor. The theory of critical distances to predict static strength of notched brittle components subjected to mixed-mode loading. *Engineering Fracture Mechanics*, 75:534–550, 2008.

[10] V. Lazarus, F.G. Buchholz, M. Fulland, and J. Wiebesiek. Comparison of predictions by mode II or mode III criteria on crack front twisting in three or four point bending experiments. *International Journal of Fracture*, 153:141–151, 2008.

[11] W.G. Knauss. An observation of crack propagation in anti-plane shear. *International Journal of Fracture Mechanics*, 6:183–187, 1970.

[12] Z. Yosibash, E. Priel, and D. Leguillon. A failure criterion for brittle elastic materials under mixed-mode loading. *International Journal of Fracture*, 141:291–312, 2006.

[13] Z. Yishu. Experimental study on mixed mode crack propagation. *Engineering Fracture Mechanics*, 34:891–899, 1989.

[14] M. L. Cooke and D. D. Pollard. Fracture propagation paths under mixed mode loading within rectangular blocks of polymethyl methacrylate. *Journal of Geophysical Research*, 101:3387–3400, 1996.

[15] J.R. Yates and K.J. Miller. Mixed mode (I + III) fatigue thresholds in a forging steel. *Fatigue Fract. Eng. Mater. Struct*, 12:259–270, 1989.

[16] M.A. Hussain, S. L. Pu, and J. Underwood. Strain energy release rate for a crack under combined mode I and mode II. *Fracture analysis, Proceedings of the 1973 National Symposium on Fracture Mechanics*, 560:2–28, 1973.

[17] V. Lazarus and J.B. Leblond. Crack paths under mixed mode (I+III) or (I+II+III) loadings. *Comptes Rendus de l'Acadmie des Sciences, Srie II*, 326:171–177, 1998.

[18] J. Chang, J. Xu, and Y. Mutoh. A general mixed-mode brittle fracture criterion for cracked materials. *Engineering Fracture Mechanics*, 73:1249–1263, 2006.

[19] S. Khan and M. Khraisheh. Analysis of mixed mode crack initiation angles under various loading conditions. *Engineering Fracture Mechanics*, 67:397–419, 2000.

[20] B. Lin, M. E. Mear, and K. Ravi-Chandar. Criterion for initiation of cracks under mixed-mode I + III loading. *International Journal of Fracture*, 165:175–188, 2010.

[21] K.H. Pham and K. Ravi-Chandar. Further examination of the criterion for crack initiation under mixed-mode I+III loading. *International Journal of Fracture*, 189:121–139, 2014.

[22] B.R. Davis, P.A. Wawrzynek, C.G. Hwang, and A.R. Ingraffea. Decomposition of 3-D mixed-mode energy release rates using the virtual crack extension method. *Engineering Fracture Mechanics*, in press, 2014.

[23] F.G. Buchholz, A. Chergui, and H.A. Richard. Fracture analyses and experimental results of crack growth under general mixed mode loading conditions. *Engineering Fracture Mechanics*, 71:455–468, 2004.

[24] P.W. Claydon. Maximum energy release rate distribution from a generalized 3D virtual crack extension method. *Engineering Fracture Mechanic*, 42:961–969, 1992.

[25] Z. Yosibash. *Singularities in Elliptic Boundary Value Problems and Elasticity and their Connection with Failure Initiation*. Springer, 2011.

[26] Z. Yosibash, N. Omer, M. Costabel, and M. Dauge. Edge stress intensity functions in polyhedral domains and their extraction by a quasidual function method. *International Journal of Fracture*, 136:37–73, 2005.